COMMUNICATION

Check for updates

Protecting Li-metal anode with LiF-enriched solid electrolyte interphase derived from a fluorinated graphene additive†

Xiaohong Wu, [iD] *[a] Yuhao Hong,[b] Zhengang Li, [iD] [c] Junhao Wang,[c] Haitang Zhang,[c] Yu Qiao, [iD] [c] Hongjun Yue*[d] and Chunhai Jiang*[a]

As the holy-grail material, the Li-metal anode has been considered the potential anode of the next generation of Li-metal batteries (LMBs). However, issues of undesirable dendrite growth and unsatisfactory reversibility of the Li-plating/stripping process during the electrochemical cycling impede further application of LMBs. Herein, we innovatively introduce fluorinated graphene (F-Gr) species as a sacrificial effective electrolyte additive into EC/EMC-based electrolyte, which effectively triggers LiF-enriched (composition) and organic/inorganic species uniform-distributed (structure) SEI film architecture that features robustness and denseness, as well as good stability. With the F-Gr additive, efficient Li-metal anode protection (dendrite-free morphology on Li-metal surface and improved Li plating/stripping reversibility during electrochemical cycling) and significantly enhanced long-term lifespan of LMBs is achieved. Remarkably, classical electrochemical techniques, combined with the surface-sensitive characterizations (XPS and TOF-SIMS), comprehensively and systematically highlight critical structure–activity relationships between the SEI architecture (both composition and structure) and electrochemical performance. These techniques provide deep insights into the optimal electrolyte designation of Li-metal anode in LMBs.

*[a]Fujian Provincial Key Laboratory of Functional Materials and Applications, Institute of Advanced Energy Materials, School of Materials Science and Engineering, Xiamen University of Technology, Xiamen, 361024, P. R. China.
E-mail: xiaohongwu@xmut.edu.cn, chjiang@xmut.edu.cn*
[b]Innovation Laboratory for Sciences and Technologies of Energy Materials of Fujian Province (IKKEM), Xiamen, 361024, P. R. China
[c]State Key Laboratory of Physical Chemistry of Solid Surfaces, College of Chemistry and Chemical Engineering, Xiamen University, Xiamen 361005, P. R. China
*[d]CAS key Laboratory of Design and Assembly of Functional Nanostructures, and Fujian Provincial Key Laboratory of Nanomaterials, Fujian Institute of Research on the Structure of Matter, Chinese Academy of Sciences, Fuzhou 350002, P. R. China.
E-mail: hjyue@fjirsm.ac.cn*
† Electronic supplementary information (ESI) available: Supporting experimental details and figures. See DOI: https://doi.org/10.1039/d4nr02877e

Xiaohong Wu

Xiaohong Wu is currently an Associate Professor in the School of Materials Science and Engineering at Xiamen University of Technology. She earned her M. D. from the University of Chinese Academy of Sciences (UCAS) in 2019. She received her Ph.D. degree from Xiamen University in 2023. Her research interests are focused on the development of electrochemical energy storage devices, surface/interfacial electrochemistry, secondary batteries, and metal-anode protection.

Introduction

The Li-metal possesses an attractive theoretical specific energy density of 3800 mA h g^{-1} and an ultra-low potential (−3.04 V) compared to the standard hydrogen electrode. It has thus been seen as the holy-grail anode for the next generation of high energy density batteries.[1–4] However, unstable electrode/electrolyte interface, undesirable dendrite growth, and continuous parasitic reactions accelerate the failure of Li-metal batteries (LMBs) with Li-metal as the anode. It hinders the development process of Li-metal anode for practical use.[5,6]

Extensive efforts have been made to effectively protect the Li-metal anode in recent years for utilization in batteries. For example, the high-performance of CC@ZnO@Li composite anode with chemical confinement can be prepared by atomic layer deposition and Li infusion experiments, resulting in a dendrite-free Li-metal anode and a long cycling lifespan of Li/Li symmetrical cells.[7] Moreover, it is reported that the problems of large variations in volume and inferior interfacial stability during continuous ion intercalation/deintercalation can be effectively addressed by designing phosphide anodes. Such anodes may also be considered and developed for Li-metal anode modification.[8] Besides, Li-metal coating with

functional components,[9] artificial protective layers,[10] as well as electrolyte optimization,[11] have been demonstrated to be effective methods to obtain stable Li-metal anode. For further practical application and production, complex as-prepared methods and procedures pose many obstacles to realizing Li-metal anodes from coin cells to pouch cells and large-scale fabrication.[12] From the perspective of engineering, the optimization of electrolytes is more convenient and easier to operate under practical conditions (*i.e.*, moderate or extreme conditions, such as low temperature) than other methods. It is thus regarded as the most favorable and preferential strategy to efficiently realize Li-metal anode protection. Targeted designation of multifunctional or sacrificial additive-assisted electrolytes, highly concentrated (HCE) or localized highly concentrated electrolytes (LHCE), and fluorinated electrolytes have become the preferred choices for electrolyte optimization.[13–16] The aforementioned electrolyte or electrolyte additive can regulate the Li$^+$-solvated sheath configuration or be involved in the composition of interfacial components to establish a robust, dense, and flexible solid electrolyte interphase (SEI) layer. Generally, the SEI film with good quality (dense, robust, and flexible) was achieved by the electrolyte optimization strategy to obtain a reversible Li plating/stripping process or restrained dendrite growth morphology on Li-metal surface to achieve desirable Li-metal protection.[17–19] However, the structural–activity relationship and the corresponding mechanism between the architecture (both composition and structure) of the SEI film and the electrochemical performance of the LMBs have not been comprehensively revealed yet.

In this work, we innovatively introduce a certain amount of fluorinated graphene (F-Gr) as an effective electrolyte additive to the EC/EMC-based electrolyte of LMBs. The F-Gr can be involved in regulating the architecture (both composition and structure) of the SEI film and effectively protect the Li-metal anode from dendrite growth and failure. With the electrolyte additive of F-Gr, the cycling stability of the Li-metal anode has been significantly enhanced. The proposed electrolyte additives modification strategy for Li-metal anode protection is an engineering-based strategy that is simple and easy to implement. Moreover, based on the F-Gr addition, we deeply and comprehensively demonstrate the structure–activity relationship between the SEI film architecture (both composition and structure) and the electrochemical performance of the LMBs, providing a new direction for the design of innovative electrolyte additives.

Results and discussion

Herein, F-Gr with a F/C molar ratio close to 1 is selected. Front and side views of the corresponding ball-and-stick models of the F-Gr are shown in Fig. S1.† Characterized with unique nanostructure and C–F bonds, F-Gr not only holds the properties of graphene (two-dimensional layer structure), but also possesses the characteristics of fluorine-based materials, such as excellent thermal and chemical stability, wide bandgap,

good mechanical strength, and larger interlayer distance as compared to the pristine graphene as a typical and popular two-dimensional atomic crystal material.[20,21] The morphology of F-Gr by SEM characterization is represented in Fig. S2,† which exhibits a typical and clear lamellar structure. Concentration optimization is considered preferentially for F-Gr as the electrolyte additive. Fig. S3a† presents the cycling performance of Li/Li symmetrical cells with different concentrations of F-Gr. With the progress of the discharge/charge cycling (almost 400 hours, Fig. S3b†) at the current density of 0.5 mA cm^{-2}, the overpotential of Li/Li symmetrical cell in the base electrolyte increases gradually. The enhanced polarization then accelerates the cell's failure in the base electrolyte. However, Li/Li symmetrical cells with F-Gr-containing electrolytes can continue to run smoothly, indicating good cycling stability. Specifically, at lower concentrations of F-Gr species, the corresponding overpotential of the Li/Li symmetrical cell is also much lower. Herein, an abbreviation of F-Gr-1 represents the addition of 1 mg F-Gr species in 1 mL of base electrolyte, while F-Gr-3 indicates 3 mg mL^{-1} F-Gr in the base electrolyte. Keeping in mind the insulting nature of F-Gr,[22] too much addition may hurt the conductivity of the electrolyte, which then affects the migration of Li$^+$ in the electrolyte and results in large polarization during cell cycling. Therefore, in this work, a low concentration of F-Gr (1 mg mL^{-1}) is selected as the optimal concentration and referred to as F-Gr.

Electrochemical performances of Li/Li symmetrical cell without (gray trace)/with (blue trace) F-Gr additive and plating capacity of 0.5 mA h cm^{-2} are exhibited in Fig. 1a. It presents rapid polarization after cycling for nearly 200 hours in the base electrolyte. Conversely, in F-Gr-containing electrolytes, significant polarization is only shown until around 300 hours. Further increase in the deposition capacity of Li/Li symmetrical cell to 1.0 mA h cm^{-2}, makes the difference in cycling stability between base and F-Gr-contained electrolyte more obvious. Excellent performance of long lifespan and stable cycling stability in electrolytes with F-Gr addition can be seen in Fig. 1b. Particularly, the morphology of the cycled Li-metal (1 mA cm^{-2}, 1 mA h cm^{-2}, 50 cycles) in Li/Li symmetrical cells with/without F-Gr are characterized by a scanning electron microscope (SEM) as shown in Fig. 1c and d. Corresponding magnified SEM images for more clear analysis are represented in Fig. S4a and S4b,† respectively. Dendritic and mossy Li on Li-metal surface is obvious and inevitable in base electrolytes, resulting in safety hazards and accelerated cell failure. There are also many cracks on the rough surface of cycled Li-metal, which may lead to continuous parasitic reactions between the fresh Li-metal and electrolyte. The deterioration of Li-metal surface morphology in the base electrolytes is not conducive to the long-term cycling of Li/Li symmetrical cells, leading to poor electrochemical performance at a certain current density (Fig. 1a and b, gray trace). However, in the F-Gr-contained electrolyte, no obvious dendrite growth can be observed on the cycled Li-metal surface (Fig. 1d and S4b†). The surface of cycled Li-metal is relatively flat and compact, which maintains the integrity of the cycled Li-metal. Hence, the long-term and
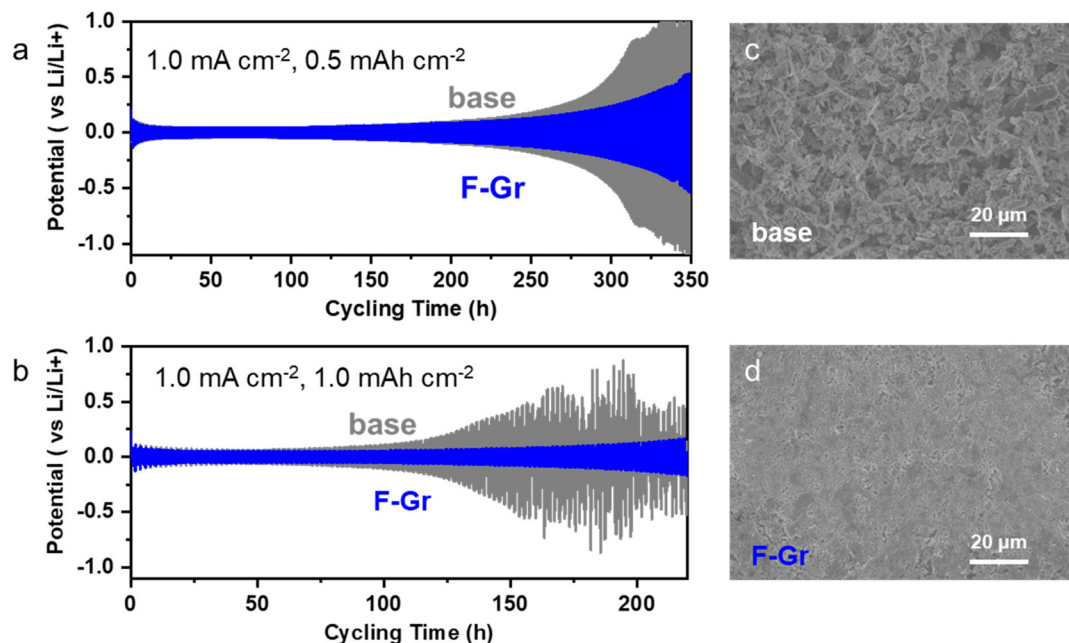
Fig. 1 Electrochemical performance of Li/Li symmetrical cell with the plating capacity of (a) 0.5 mA h cm^{-2} and (b) 1.0 mA h cm^{-2}, respectively (base: gray trace; F-Gr: blue trace). SEM images of the Li-metal surface in the electrolyte (c) without and (d) with F-Gr after 50 cycles at the current density of 1 mA cm^{-2}.

stable cycling performance of Li/Li symmetrical cells in F-Gr-contained electrolytes can be realized under different testing conditions (Fig. 1a, b and S3,† blue trace). Furthermore, the deposition morphology of Li on Cu substrate with/without F-Gr from plated Li-metal at a plating capacity of 2.0 mA h (current: 0.01 mA) is represented in Fig. S5.† A rough and uneven surface with cracks results in continuous dendrite growth and the accumulation of dendrites can be observed on the Li-metal surface without F-Gr. However, a relatively flat surface with no significant dendrite growth on Li-metal can be obtained with F-Gr. The significant difference in the deposition morphology of Li on Cu substrate further indicates that the introduction of the F-Gr additive can effectively suppress detrimental and undesirable dendritic growth, thereby enhancing the cycling stability of Li/Li symmetrical cells with F-Gr. In ether-based electrolytes (BASE, 1.0 M LiTFSI in TEGDME), F-Gr can still work in significantly enhancing the cycling performance of Li/Li symmetrical cells under Ar environment and effectively suppresses detrimental dendrite growth (Fig. S6 and S7,† respectively). Herein, we focus our research just on the working mechanism of F-Gr in an ester electrolyte (1.0 M LiPF$_6$ in EC/EMC), rather than in the ether electrolyte.

To explore the reason behind the significantly enhanced cycling stability of Li/Li symmetrical cells with F-Gr, and whether the F-Gr additive has altered the composition of SEI film at Li-metal/electrolyte interface, X-ray photoelectron spectroscopy (XPS) is preferentially conducted as an ideal surface-sensitive technique to analyze Li-metal surface.[23] Ar$^+$ sputtering was directly conducted to probe the compositional changes in the SEI layer at different etching depths. Generally,

the peak intensity of XPS spectra can be utilized to evaluate the relative content of species because no additional and redundant processing has been done on the original spectra. Notably, when the scale bar of XPS spectra (Y axis, peak intensity) remains the same, the height of the peak can be used to approximate the content of the corresponding substance.[24] From O 1s spectra, the peak centered at 532.0 eV in Fig. 2a can be assigned to carbonate species (Li$_2$CO$_3$). As exhibited, according to XPS characterization, the total amount (*i.e.*, the sum of the amount of both inner and outer layers) of Li$_2$CO$_3$ species in the F-Gr-contained electrolyte is relatively much lower than that in the base electrolyte. Since Li$_2$CO$_3$ is mainly derived from electrolyte decomposition, especially the solvent in EC/EMC-based electrolytes with or without F-Gr, the difference in the total amount of Li$_2$CO$_3$ between the base and F-Gr-containing electrolyte reveals that electrolyte decomposition-related parasitic reactions have been effectively suppressed with F-Gr introduction. The binding energy of 530.3 and 528.1 eV indicates LiOH (green region) and Li$_2$O (orange region) species, respectively, which may be derived from the chemical parasitic reactions between Li-metal and side products of electrolyte electrochemical/chemical decomposition, such as H$_2$O and O$_2$.[25,26] The amount of LiOH can usually be used to evaluate the corrosion degree of Li-metal, which is the main component of the detrimental surface corrosion layer on the Li-metal anode.[27] Li$_2$O is also inseparable from the failure of Li-metal during cycling. As the etching depth increases from 0 to 20 nm (Fig. 2a), the content of LiOH and Li$_2$O species on cycled Li-metal (1 mA cm^{-2}, 1 mA h cm^{-2}, 50 cycles) with base electrolyte are significantly higher than that with F-Gr. On the
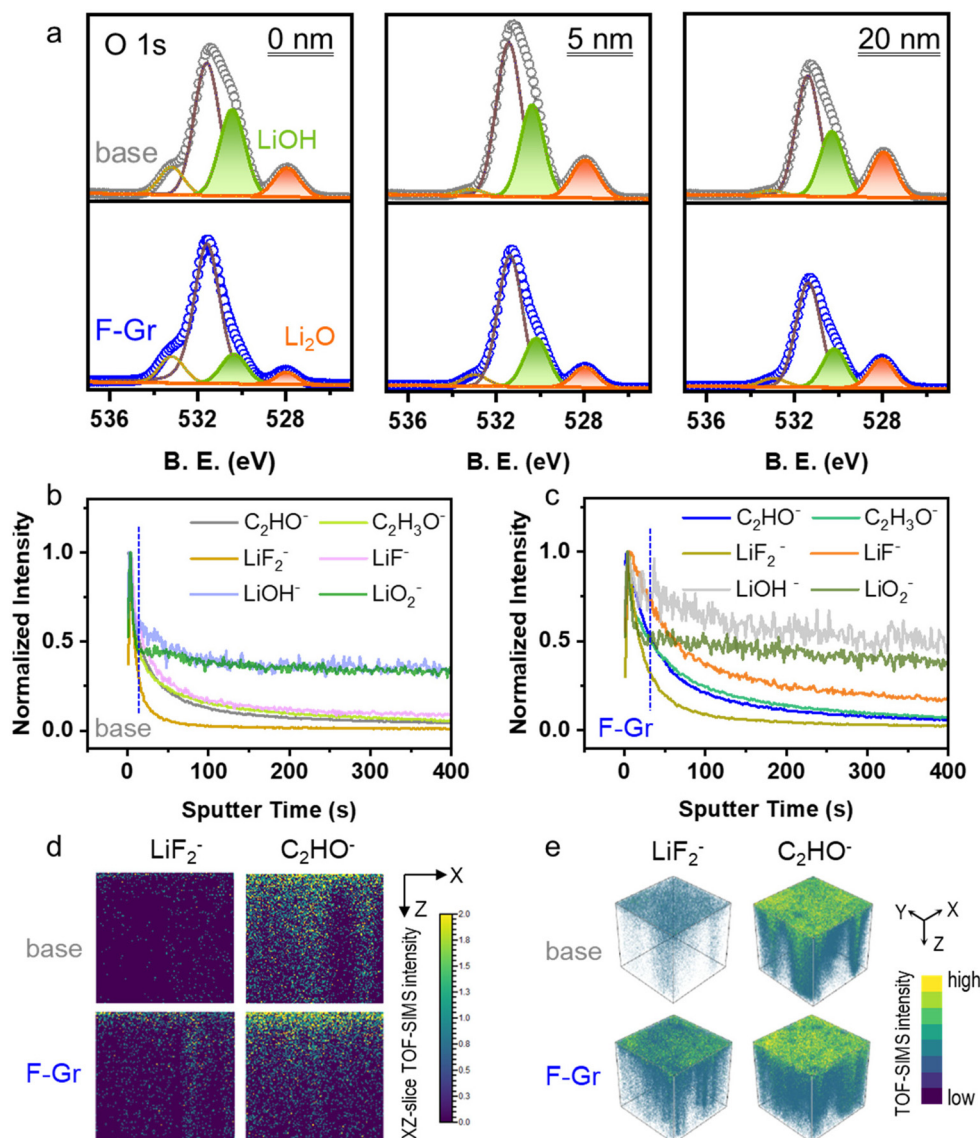
Fig. 2 Surface characterizations of cycled Li-metal in base and F-Gr-contained electrolyte. (a) O 1s spectra for Li-metal cycled in base or F-Gr-contained electrolyte with a sputtering depth of 0, 5, 20 nm. The Li-metal is retrieved from the Li/Li symmetrical cell after 50 cycles, which is cycled at 1.0 mA cm^{-2} with a fixed plating capacity of 1.0 mA h cm^{-2}. TOF-SIMS depth profiles of cycled Li-metal (1 mA cm^{-2}, 1 mA h cm^{-2}, 50 cycles) with (b) base electrolyte and (c) F-Gr-contained electrolyte in spectrometry negative-ion mode, respectively. (d) The intuitive 2D plane reconstructed images in the *XZ* direction of typical ion fragments. (e) TOF-SIMS 3D renders images of the Li-metal surface after the electrochemical cycling process in the base and F-Gr-contained electrolyte.

one hand, a relatively larger amount of LiOH or Li$_2$O in the SEI film is detrimental to the long-term stable cycling of the Li-metal anode. Moreover, it indicates that more electrolyte decomposition-related parasitic reactions occur in base electrolytes, rather than in F-Gr-contained electrolytes. Hence, we can conclude that the introduction of F-Gr in electrolytes has significantly inhibited side reactions related to electrolyte decomposition and alleviated the corrosion of Li-metal anode, which promotes the cycling stability of Li-metal. F 1s spectra of XPS in Fig. S8† further indicate that a higher amount of LiF species exists in the SEI layer at different depths with F-Gr additive than with the base electrolyte.

To obtain more insight into the SEI architecture regarding the three-dimensional distribution of the Li-metal, the time-of-flight secondary-ion mass spectrometry (TOF-SIMS) technique with superior lateral and depth resolutions, as well as high sensitivity, was applied.[28] Herein, at least two specific secondary ions rather than single secondary ions of key substance were selected and assigned for comprehensive analysis and interpretation. Fig. 2b and c show the TOF-SIMS depth profiles with the normalized intensity of cycled Li-metal (1 mA cm^{-2}, 1 mA h cm^{-2}, 50 cycles) in the base and the F-Gr-containing electrolytes, respectively. Secondary ions of C$_2$HO$^-$ and C$_2$H$_3$O$^-$ represent the typical organic species in the SEI layer

induced by the decomposition of the organic solvent molecule, while LiF_2^- and LiF^- secondary ions assign the typical inorganic species of LiF in the SEI film. In the depth profiles exhibited in Fig. 2b and c, a slightly thicker SEI layer in the F-Gr-containing electrolyte than in the base electrolyte can be obtained. The depth curves in Fig. S9† with intensity also demonstrate a thinner SEI film in the base electrolyte. Moreover, a combination of depth profiles (Fig. 2b, c, and S9†), 2D-*XZ* plane reconstructed images (Fig. 2d and S10†), and 3D visualizations (Fig. 2e and S11†) were utilized to comprehensively demonstrate the specific stratified architecture of the SEI with/without F-Gr additive in the base electrolyte. Salient characteristics can be summarized when the SEI film is compared. The SEI layer formed in the base electrolyte is mainly composed of organic species. In the F-Gr-containing, organic and inorganic species make up the SEI configuration together, which is confirmed by the similar signal intensity without significant difference of the C_2HO^- and LiF_2^- in the F-Gr-containing electrolyte than in the base electrolyte (Fig. S9†). Furthermore, in base electrolytes, inorganic species are dominant in the outer layer of the SEI film. Organic components run through the entire SEI layer but are unevenly distributed in the inner layer, which is observed from the 2D image (Fig. 2d) and a 3D view (Fig. 2e) in the base electrolytes. However, comparatively uniformly distributed inorganic and organic species throughout the SEI layer can be observed in F-Gr-containing electrolytes than in the base electrolytes (Fig. S9, S10 and S11†), which promotes a uniform SEI architecture in the electrolytes with F-Gr. It can ensure a rapid migration of Li^+ in the interfacial SEI layer, which is more conducive to the interfacial stability between the Li-metal and electrolyte. Hence, with the F-Gr additive, it exhibits long and stable cycling performance of Li/Li symmetrical cell and cycled Li-metal morphology is well maintained, as shown in Fig. 1a, b, and d, respectively. Notably, the ion fragments of $LiOH^-$ and LiO_2^- represent LiOH and LiO_2 components on the Li-metal surface, respectively. The significant intensity and distribution difference in Fig. S10 and S11† about $LiOH^-$ and LiO_2^- fragments between the base and F-Gr-contained electrolytes indicate that there are more pronounced and concentrated distributions of LiOH and Li_2O species in the base than in the F-Gr-containing electrolytes, which are consistent with the characterizations and discussions on the O 1s spectra of the XPS (Fig. 2a).

To further comprehensively investigate the reason for the difference in SEI film architecture between the base and F-Gr-containing electrolytes, a series of typical electrochemical characterizations were performed. Cyclic voltammetry (CV) profiles in the range of 2.5–0.0 V at a scan rate of 1.0 mV s^{-1} were measured by Li/Cu asymmetric cell with/without F-Gr additive (base: gray trace; F-Gr: blue trace) as shown in Fig. 3a. Corresponding profiles extended by time-current density are exhibited in Fig. 3b. Herein, the region of the CV curve enclosed by the *X*-axis between 2.0 and 0.0 V during the cathodic scan is assigned to SEI formation (marked as orange part), and the profile after 0.0 V is classified as possible SEI

decomposition during the anodic scan (designated by purple part). A weaker current density response can be observed in the F-Gr-containing electrolyte than in the base electrolyte during both SEI formation and possibly the decomposition part. It indicates that restrained electrolyte reduction and weaker SEI decomposition occurred in the F-Gr-containing electrolytes, resulting in suppressed electrolyte-related parasitic reactions and well-maintained SEI architecture during continuous electrochemical cycling. These observations are in good agreement with the characterizations and discussions by XPS and TOF-SIMS in Fig. 2. Notably, a new peak appears in the SEI formation region with the F-Gr additive. Compared with the component difference between base and base electrolyte with the F-Gr additive, the new peak reveals a preferential reduction of F-Gr, which is highlighted by a green quadrangle both in Fig. 3a and b. During the SEI formation region, the reductive decomposition of F-Gr contributes to the SEI components of LiF, that is, F-Gr participates in the construction of SEI films architecture. Hence, although the decomposition of electrolytes is significantly inhibited, the amount of LiF species increases in the F-Gr-containing electrolyte, corresponding to the F 1s spectra shown in Fig. S8.†

Generally, the Li plating/stripping reversibility can significantly affect the cycling stability of the Li-metal. CV test with 2 cycles was performed by Li/Cu half-cell with a cut-off voltage window in the range of −0.3 to 0.6 V at a scan rate of 1 mV s^{-1}. As shown in Fig. 3c, the stripping peak area in an F-Gr-containing electrolyte is much larger than that in the base electrolyte as the plating peak area is similar at the first cathodic and anodic scan. This reveals a higher plating/stripping efficiency with the F-Gr additive. At the second cycle (Fig. S12†) or at the higher scan rate of 10 mV s^{-1} (Fig. S13†), enhanced and higher reversibility during the plating/stripping process can also be observed in the F-Gr-contained electrolyte, which promotes long-term cycling stability of Li/Li symmetrical cell with the F-Gr additive (Fig. 1a and b). Furthermore, the linear sweep voltammetry (LSV) measurement was conducted to investigate the oxidation stability of electrolytes with/without F-Gr (Fig. 3d). Undesirable oxidation peaks can be observed in the base electrolyte (gray trace), which can induce deterioration of battery performance and is detrimental to the cell's long-term cycling. Conversely, enhanced oxidation stability is exhibited in F-Gr-containing electrolytes (blue trace), which can significantly reduce unnecessary electrolyte-related side reactions and promote long-term stable cycling performance of the battery. Resistance of Li^+ transportation through the SEI film (R_{SEI}) in Li/Li symmetrical cells after a certain number of cycles (25, 50, and 100 cycles) by electrochemical impedance spectroscopy (EIS) technique is demonstrated and summarized in Fig. 3e. Origin EIS curves in EC/EMC-based electrolytes with/without F-Gr are represented in Fig. S14.† With the progress of electrochemical cycling, the R_{SEI} value remains relatively stable with the F-Gr additive; it is always lower than that with the base electrolyte. It indicates that the SEI film architecture in F-Gr-contained electrolyte is more conducive to the migration of Li^+, which is attributed to the formation of excel-
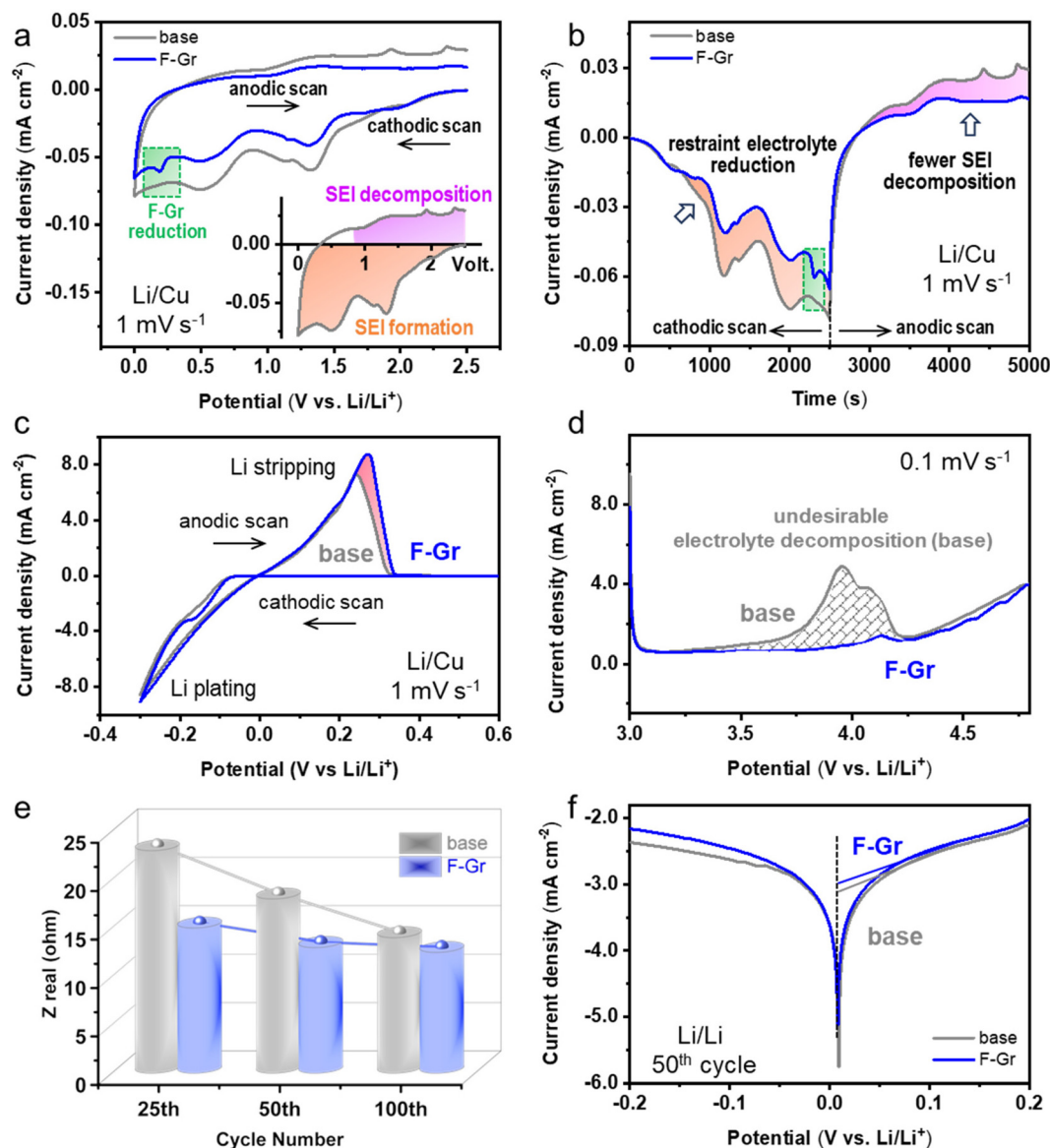
Fig. 3 Comparison of the (a) cyclic voltammetry (CV) curves between the base and F-Gr-containing electrolyte. Scan rate: 1 mV s^{-1}; voltage range: 2.5 to 0.0 V. The magnified profile before 0 V can be assigned to the SEI formation process (marked by orange region) and SEI decomposition process after 0 V (marked by purple region), respectively. (b) Cyclic voltammetry curve extended by time (X-axis) without/with F-Gr. The critical point of the cathodic−anodic scan and preferential decomposition peak of F-Gr have been highlighted. (c) CV curves by Li/Cu half-cells during the Li plating/stripping process with/without F-Gr. (d) Comparison of LSV profiles between base and F-Gr-contained electrolytes with a scan rate of 0.1 mV s^{-1}. Base: gray trace; F-Gr: blue trace. (e) Li$^+$ transportation resistance through the SEI film for cycled Li/Li symmetrical cells (25, 50, 100 cycles) with/without F-Gr (0.5 mA cm^{-2}, 0.5 mA h cm^{-2}). (f) Tafel plots of cycled Li/Li symmetrical cells in different electrolytes (0.5 mA cm^{-2}, 0.5 mA h cm^{-2}).

lent SEI architecture (LiF-enriched, organic/inorganic species even-distributed) at Li-metal/electrolyte interface with F-Gr as confirmed by XPS and TOF-SIMS in Fig. 2. The higher exchange current density in the Tafel curve (Fig. 3f) further validates and confirms the faster migration dynamics at the Li-metal/electrolyte interface with the F-Gr additive than that at the base electrolyte.[29,30] Based on the XPS and TOF-SIMS measurements, as well as electrochemical techniques, we can conclude that the SEI film architecture was characterized by abundant LiF and uniformly distributed organic and inorganic

species is prominently dense and electrochemical/chemical stable, which can significantly promote Li$^+$ migration dynamics and enhance Li plating/stripping reversibility. Importantly, it can effectively keep the configuration intact during continuous electrochemical cycling and avoid fragmental accumulation, resulting in restrained electrolyte decomposition and long-term battery performance.

To further investigate the feasibility of the F-Gr additive, the cycling performance of Li/LiNi$_{0.8}$Co$_{0.1}$Mn$_{0.1}$O$_2$ (NCM 811) batteries was studied. In Fig. 4a, the Li/NCM 811 battery with F-Gr
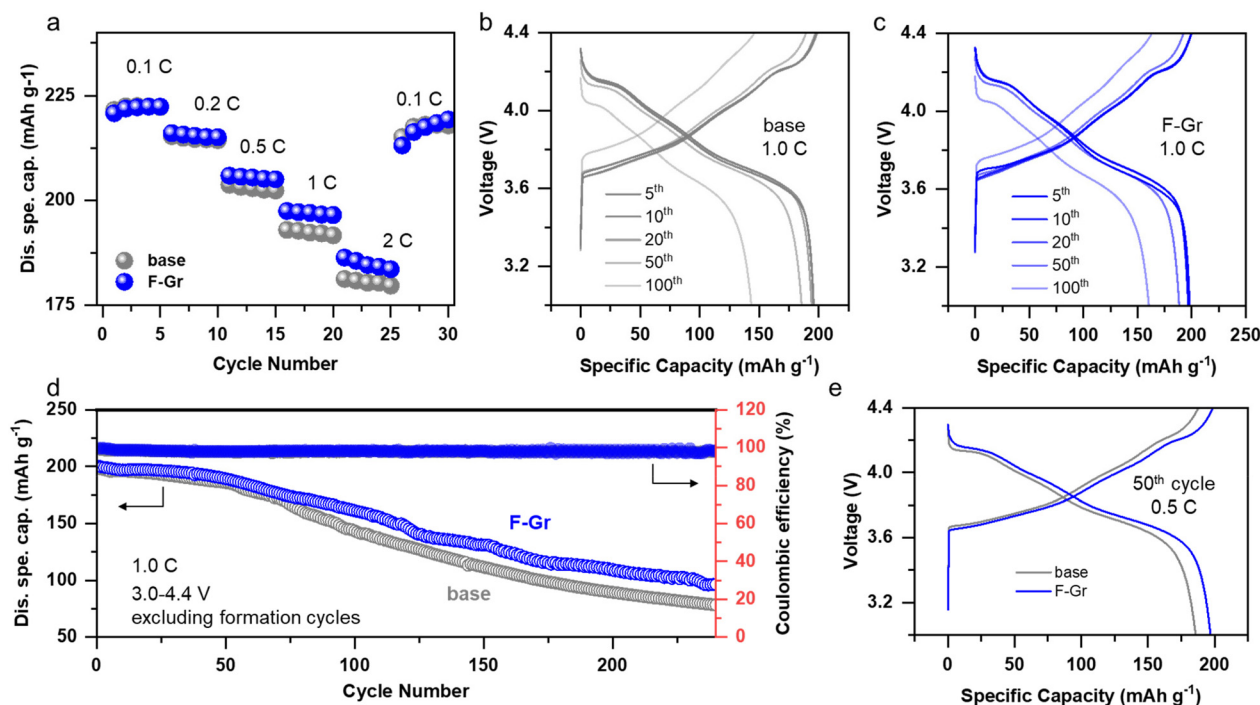
Fig. 4 Comparison of the (a) long-term cycling stability at 1.0 C charge/discharge after 3 activation cycles at 0.1 C between 3.0 and 4.4 V and (b) rate capability of coin-type Li/NCM811 batteries with/without F-Gr additive (base: gray trace; F-Gr: blue trace). Galvanostatic charge/discharge profiles of Li/NCM811 batteries in (c) base electrolyte and (d) F-Gr-contained electrolyte, respectively. (e) The comparison of the charge/discharge curve at the 50th cycle (base: gray trace; F-Gr: blue trace) at 0.5 C.

outperforms that with the base electrolyte in rate capability, which is attributed to accelerated Li$^+$ migration at the Li-metal/electrolyte interface promoted by the dense and uniform SEI layer in F-Gr-contained electrolyte. Fig. 4b and c illustrate the typical galvanostatic discharge–charge profiles of Li/NCM 811 batteries at 1.0 C without and with F-Gr additive, respectively. It can be observed from the discharge capacity evolution at a cut-off voltage of 3.0 V that with the cycling progress, a serious capacity decline of Li/NCM 811 battery exists in the base electrolyte. Specifically, in Fig. 4d, the Li/NCM 811 battery with base electrolyte starts to degrade after 75 cycles and exhibits a low capacity of 145 mA h g^{-1} with a capacity retention of 72.5% after 100 cycles, which shows rapid capacity decay. Conversely, the Li/NCM 811 battery with F-Gr represents effectively suppressed deterioration and excellent and stable cycling performance, which delivers 163 mA h g^{-1} at 1.0 C with a cut-off voltage window in the range of 3.0 to 4.4 V after 100 cycles. Generally, the consumption of active Li$^+$ due to parasitic reactions between fresh Li-metal and electrolyte, as well as loss of active material in the Li-metal anode, can inevitably cause capacity degradation in batteries.[31,32] With the F-Gr additive, electrolyte-related side reactions have been effectively restrained and the reversibility of the Li plating/striping process has been significantly enhanced, which boosts the stable cycling performance of the Li/NCM 811 battery. The comparison of the charge–discharge curves of the 50th cycle at 0.5 C (Fig. 4e) further verifies the phenomenon of capacity

degradation and deterioration of Li/NCM 811 battery in the base electrolyte, which is detrimental to long-term stable cycling. Furthermore, the self-discharge behavior of Li/NCM811 cells caused by electrolyte decomposition can be significantly suppressed by the F-Gr introduction as represented in Fig. S15.†

Conclusions

In summary, we have demonstrated the electrolyte engineering involving fluorinated graphene (F-Gr) additive for efficient Li-metal protection and enhanced long-term cycling performance of LMBs. F-Gr prevents sacrificial decomposition and participates in the construction and regulation of the SEI layer, resulting in LiF-enriched (composition) and organic/inorganic species uniform-distributed (structure) SEI layer architecture characterized by high density, robustness, and good stability. It has been comprehensively confirmed by surface-sensitive technology of XPS and TOF-SIMS characterizations. Moreover, a series of typical and basic electrochemical techniques sufficiently verify such SEI layer architecture with high quality (composition and structure) as the aforementioned can result in corresponding electrochemical behaviours of fast dynamics of Li+ migration at the Li-metal/electrolyte interface and restraint electrolyte-related parasitic reactions during electrochemical cycling. XPS, TOF-SIMS characterizations, and

electrochemical techniques have built a bridge between SEI layer architecture and electrochemical performance, which comprehensively and systematically reveal the structure–activity relationship between SEI layer architecture and electrochemical performance. It can shed light on the additive designation of electrolyte optimization for Li-metal protection in LMBs.

Author contributions

X. W., Y. Q., H. Y., and C. J. contributed to the design of the research and performed the experimental data analysis. X. W. conducted the electrochemical characterization. Y. H. performed TOF-SIMS characterization. Z. L. performed the SEM characterization, and J. W. conducted the XPS characterizations. H. Zhang performed the Li/NCM 811 test. All authors co-wrote the manuscript. X. W., Y. Q., H. Y., and C. J. supervised the work. All authors discussed the results and commented on the manuscript.

Data availability

The data in this article ("Protecting Li-metal anode with LiF-enriched solid electrolyte interphase derived from a fluorinated graphene additive") have been plotted with the Origin software and can be reproduced repeatedly. The data supporting this article have been included as part of the ESI.†

Conflicts of interest

The authors declare no conflict of interest.

Acknowledgements

References

1 A. J. Sanchez and N. P. Dasgupta, *J. Am. Chem. Soc.*, 2024, **146**, 4282–4300.

2 X. He, K. Zhang, Z. Zhu, Z. Tong and X. Liang, *Chem. Soc. Rev.*, 2024, **53**, 9–24.

3 X. B. Cheng, S. J. Yang, Z. Liu, J. X. Guo, F. N. Jiang, F. Jiang, X. Xiong, W. B. Tang, H. Yuan, J. Q. Huang, Y. Wu and Q. Zhang, *Adv. Mater.*, 2024, **36**, 2307370.

4 F. Qiu, S. Ren, X. Zhang, P. He and H. Zhou, *Sci. Bull.*, 2021, **66**, 897–903.

5 K. Pan, L. Zhang, W. Qian, X. Wu, K. Dong, H. Zhang and S. Zhang, *Adv. Mater.*, 2020, **32**, 2000399.

6 X. B. Cheng, R. Zhang, C. Z. Zhao and Q. Zhang, *Chem. Rev.*, 2017, **117**, 10403–10473.

7 H. Qiao, X. Li, Q. Chen, W. Liu, Z. Zhao, Z. Ma, Y. Cao, J. Wang, W. Li, K. Xu, K. Zhang, W. Yan, J. Zhang and X. Li, *Adv. Funct. Mater.*, 2024, **34**, 2310143.

8 Y. Hao, J. Shao, Y. Yuan, X. Li, W. Xiao, H. Sari, T. Liu and J. Lu, *Adv. Funct. Mater.*, 2023, **33**, 2212692.

9 G. Lu, J. Nai, D. Luan, X. Tao and X. W. Lou, *Sci. Adv.*, 2023, **9**, eadf1550.

10 X. He, Z. Liu, Y. Yang, Z. Wang, Y. Chen, Q. Zhang, Z. Shi, Y. Tan, X. Yue and Z. Liang, *J. Mater. Chem. A*, 2023, **11**, 10155–10163.

11 X. Zhang, X. Fu, W. Tian, Y. Bai, L. Zhu and J. Si, *Nanoscale*, 2023, **15**, 15328–15333.

12 Q. Wang, T. Lu, Y. Xiao, J. Wu, L. Guan, L. Hou, H. Du, H. Wei, X. Liu, C. Yang, Y. Wei, H. Zhou and Y. Yu, *Eletrochem. Energy Rev.*, 2023, **6**, 22.

13 S. Tan, Z. Shadike, X. Cai, R. Lin, A. Kludze, O. Borodin, B. L. Lucht, C. Wang, E. Hu, K. Xu and X.-Q. Yang, *Eletrochem. Energy Rev.*, 2023, **6**, 35.

14 H. Zhang, G. G. Eshetu, X. Judez, C. Li, L. M. Rodriguez-Martinez and M. Armand, *Angew. Chem., Int. Ed.*, 2018, **57**, 15002–15027.

15 Y.-N. Li, F.-L. Jiang, Z. Sun, O. Yamamoto, N. Imanishi and T. Zhang, *ACS Appl. Mater. Interfaces*, 2021, **13**, 16437–16444.

16 Y. Wang, Z. Li, Y. Hou, Z. Hao, Q. Zhang, Y. Ni, Y. Lu, Z. Yan, K. Zhang, Q. Zhao, F. Li and J. Chen, *Chem. Soc. Rev.*, 2023, **52**, 2713–2763.

17 X. Zhang, J. Zhang, M. Jia, L. Peng, N. Zhang, S. Qi and L. Zhang, *Green Chem. Eng.*, 2023, **4**, 49–56.

18 Y. N. Zhang, F. L. Jiang, F. Bai, H. Jiang and T. Zhang, *ACS Appl. Mater. Interfaces*, 2022, **14**, 10327–10336.

19 Q.-K. Zhang, X.-Q. Zhang, J. Wan, N. Yao, T.-L. Song, J. Xie, L.-P. Hou, M.-Y. Zhou, X. Chen, B.-Q. Li, R. Wen, H.-J. Peng, Q. Zhang and J.-Q. Huang, *Nat. Energy*, 2023, **8**, 725–735.

20 K.-J. Jeon, Z. Lee, E. Pollak, L. Moreschini, A. Bostwick, C.-M. Park, R. Mendelsberg, V. Radmilovic, R. Kostecki, T. Richardson and E. Rotenberg, *ACS Nano*, 2011, **5**, 1042–1046.

21 L. Liao, H. Peng and Z. Liu, *J. Am. Chem. Soc.*, 2014, **136**, 12194–12200.

22 X. Wu, X. Wang, Z. Li, L. Chen, S. Zhou, H. Zhang, Y. Qiao, H. Yue, L. Huang and S. G. Sun, *Nano Lett.*, 2022, **22**, 4985–4992.

23 A. Bhargav, H. Y. Asl and A. Manthiram, *J. Mater. Chem. A*, 2023, **11**, 9772–9783.

24 X. Wu, Z. Li, C. Song, L. Chen, P. Dai, P. Zhang, Y. Qiao, L. Huang and S.-G. Sun, *ACS Mater. Lett.*, 2022, **4**, 682–691.

25 H. Luo, B. Zhang, H. Zhang, Q. Zheng, X. Wu, Y. Yan, Z. Li, Y. Tang, W. Hao, G. Liu, Y.-h. Hong, J. Ye, Y. Qiao and S.-G. Sun, *J. Phys. Chem. Lett.*, 2023, **14**, 4565–4574.

26 H. Luo, B. Zhang, H. Zhang, X. Wu, Q. Zheng, Y. Yan, Z. Li, Y. Tang, W. Hao, G. Liu, Y.-H. Hong, J. Ye, Y. Qiao and S.-G. Sun, *J. Phys. Chem. C*, 2023, **127**, 16319–16330.

27 Y. Yu, Y.-B. Yin, J.-L. Ma, Z.-W. Chang, T. Sun, Y.-H. Zhu, X.-Y. Yang, T. Liu and X.-B. Zhang, *Energy Storage Mater.*, 2019, **18**, 382–388.

28 S.-K. Otto, Y. Moryson, T. Krauskopf, K. Peppler, J. Sann, J. Janek and A. Henss, *Chem. Mater.*, 2021, **33**, 859–867.

29 Q. Yang, J. Hu, J. Meng and C. Li, *Energy Environ. Sci.*, 2021, **14**, 3621–3631.

30 S. Zhang, X. Zhuang, X. Du, X. Zhang, J. Li, G. Xu, Z. Ren, Z. Cui, L. Huang, S. Wang, F. Sun, L. Qiao, S. Dong and G. Cui, *Adv. Mater.*, 2023, **35**, e2301312.

31 S. Lee, W. Li, A. Dolocan, H. Celio, H. Park, J. H. Warner and A. Manthiram, *Adv. Energy Mater.*, 2021, **11**, 2100858.

32 J. Zhou, B. Hao, M. Peng, L. Zhang, H. Ji, J. Liu, W. Ling, C. Yan and T. Qian, *Adv. Energy Mater.*, 2023, **13**, 2204174.